

# A microfluidic device for thermal particle detection

Ashwin Kumar Vutha · Benyamin Davaji ·  
Chung Hoon Lee · Glenn M. Walker

Received: 27 August 2013 / Accepted: 17 February 2014 / Published online: 7 March 2014  
© Springer-Verlag Berlin Heidelberg 2014

**Abstract** We demonstrate the use of heat to count microscopic particles. A thermal particle detector (TPD) was fabricated by combining a 500-nm-thick silicon nitride membrane containing a thin-film resistive temperature detector with a silicone elastomer microchannel. Particles with diameters of 90 and 200  $\mu\text{m}$  created relative temperature changes of 0.11 and  $-0.44$  K, respectively, as they flowed by the sensor. A first-order lumped thermal model was developed to predict the temperature changes. Multiple particles were counted in series to demonstrate the utility of the TPD as a particle counter.

**Keywords** Microfluidics · Particle counting · Thermal

## 1 Introduction

Particle counters have been an active area of research in the microfluidics community for over a decade (Zhang et al.

2009). During this time, many particle counting strategies have been explored, but the vast majority use either electrical or optical methods for detection. Electrical, or coulter, particle counters are relatively inexpensive to fabricate and can be miniaturized, but they cannot provide detailed information about particle subpopulations and are sensitive to the working fluids that carry the particles. For example, a conventional coulter counter that measures only resistance cannot enumerate metallic particles suspended in an insulating fluid such as oil (Murali et al. 2009). Instead, changes in capacitance must be measured. In contrast, optical counters, based on the detection of fluorescently labeled tags or light scattering, can identify cell subpopulations and are exquisitely fast, but they require expensive optical components to function and are not easily miniaturized. In addition, fluorescent flow cytometers are fundamentally limited to measuring 6–10 colors, or parameters, because the optical spectra of dyes begin to overlap if more colors are used (Janes and Rommel 2011). There is a need for new particle counting approaches that are both low cost and that can identify subpopulations of particles in a heterogeneous mixture.

Of all the particle counting methods explored so far, heat remains uninvestigated. Microfabrication allows the creation of inexpensive yet sensitive thermometers that can detect minute changes in the thermal properties of a liquid within a microchannel. Since particles suspended in a fluid alter the thermal properties of that fluid, a sensitive thermometer becomes a de facto particle counter. In addition to counting, a microscale thermometer could measure the thermal properties of cells and other particles or droplets to identify and characterize them. For example, Yi et al. (2011) generated DI water droplets containing bovine serum albumin (BSA) and measured the thermal conductivity of the droplets within a microchannel. However, the

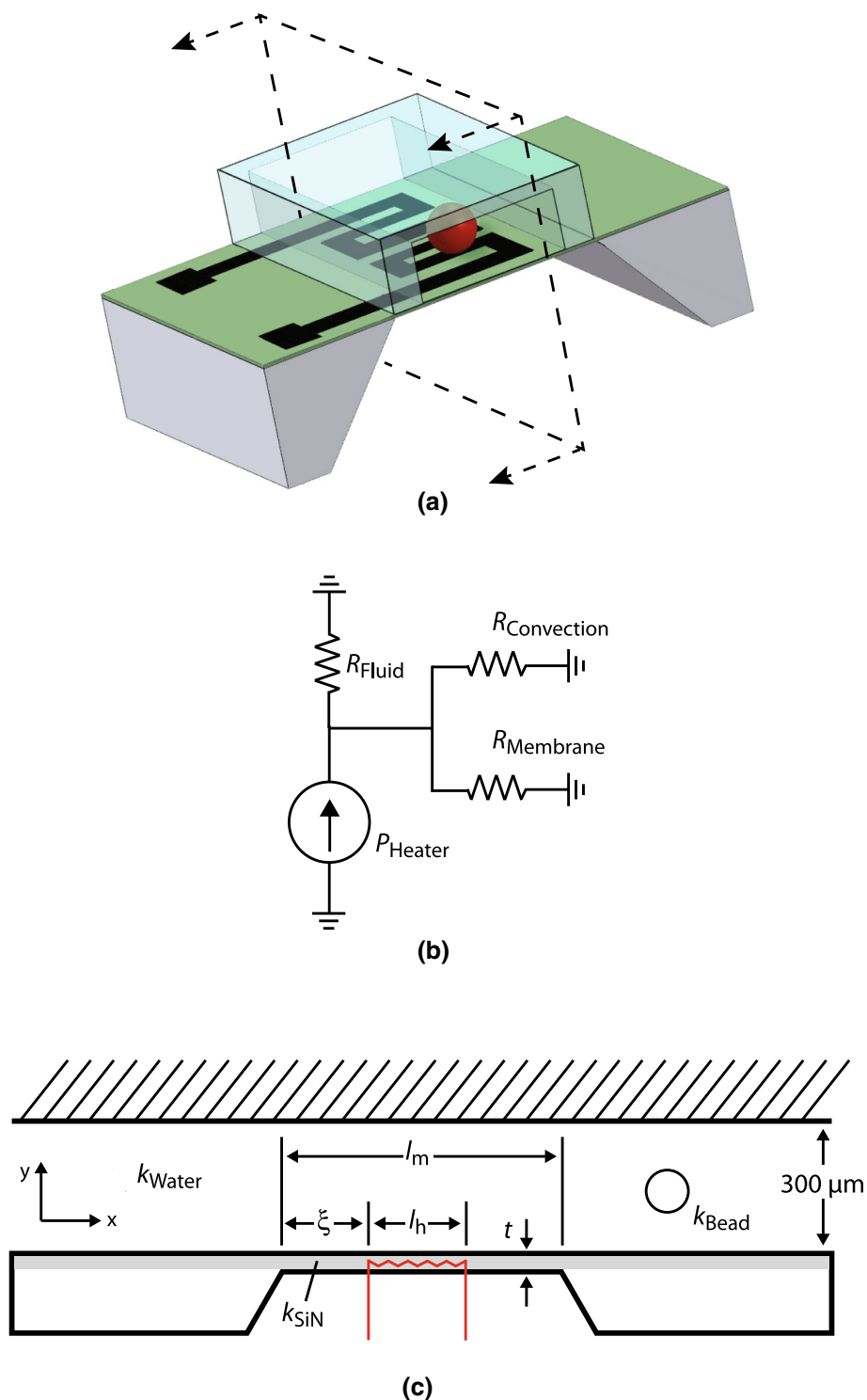
---

A.Vutha  
Department of Mechanical, Aerospace, and Nuclear  
Engineering, Rensselaer Polytechnic Institute, 2112 Jonsson  
Engineering Center, Troy, NY 12180, USA

B. Davaji · C. H. Lee  
Department of Electrical and Computer Engineering,  
Marquette University, 1515 W Wisconsin Ave., Milwaukee,  
WI 53233, USA  
e-mail: chunghoon.lee@marquette.edu

G. M. Walker (✉)  
Joint Department of Biomedical Engineering,  
UNC Chapel Hill and NC State University, 911 Oval Drive,  
Raleigh, NC 27695, USA  
e-mail: gmwalker@ncsu.edu

**Fig. 1** **a** Three-dimensional rendering of the device showing a bead passing over the sensor. **b** Heat enters the system through Joule heating of the RTD and leaves through convection and conduction through the membrane and fluid. **c** Cross-section of the device showing relevant dimensions:  $l_m = 300 \mu\text{m}$ ,  $l_h = 200 \mu\text{m}$ ,  $\xi = 50 \mu\text{m}$ ,  $t = 0.5 \mu\text{m}$



focus of their work was on characterizing the contents of liquid droplets which occupied the entire width of the channel, and not on counting particles.

In this paper, we demonstrate a thermal particle detector (TPD) that can count and quantify solid particles suspended in a liquid using only heat. A lumped thermal

model explains the observed results and predicts the effect of particle size and thermal conductivity on the detected temperature change. To demonstrate proof-of-concept, we used a microfabricated resistance temperature detector (RTD) within a microchannel to detect polystyrene microspheres.

## 2 Theory

The heat flux through a material is described by Fourier’s law of heat conduction:  $q = -k\partial T/\partial y$ , where  $q$  is heat flux ( $\text{W}/\text{m}^2$ ),  $k$  is the thermal conductivity of the material ( $\text{W}/\text{m K}$ ), and  $\partial T/\partial y$  is the temperature gradient ( $\text{K}/\text{m}$ ) along the  $y$  direction. For a heater producing a constant heat flux, an increase in the thermal conductivity of the material will decrease  $\Delta T$ , and vice versa. Therefore, Fourier’s law can be used to detect particles flowing in a microchannel if they have a different thermal conductivity than the fluid. Consider a constant heat flux from the floor of a microchannel. Even with fluid flow, the heat flux will eventually generate a steady-state temperature gradient within the microchannel. If a particle with a different thermal conductivity than the fluid passes over the heat source, as illustrated in Fig. 1a, the temperature gradient will either increase or decrease depending on the thermal conductivity of the particle. If the heater is also used as a thermometer, the heater temperature can be used to detect particles. This general principle forms the basis of the TPD.

The heat flow within the TPD can be modeled using a first-order electrical circuit analogy, as illustrated in Fig. 1b. In the circuit, the RTD generates a small amount of heat via Joule heating and is analogous to a current source, and the thermal resistances within the TPD are analogous to electrical resistances. The voltage at the node above the current source is analogous to the temperature of the heat source. Heat enters into the TPD through the RTD and exits through three routes: (1) conduction through the membrane, (2) conduction through the fluid directly above the RTD, and (3) convection within the microchannel (van der Wiel et al. 1993). Each of these routes has a thermal resistance associated with it. Using the system diagram in Fig. 1c, the thermal resistances can be calculated. The thermal resistance of the membrane is

$$R_{\text{Membrane}} = \frac{\ln(r_m/r_h)}{2\pi k_{\text{SiN}}t} \tag{1}$$

where  $r_m$  is the membrane radius ( $r_m = \sqrt{l_m^2/\pi}$ ),  $r_h$  is the heater radius ( $r_h = \sqrt{l_h^2/\pi}$ ),  $k_{\text{SiN}}$  is the thermal conductivity of the silicon nitride (SiN) membrane (16  $\text{W}/\text{m K}$ ), and  $t$  is the membrane thickness (Lee et al. 2008).

The thermal resistance of the hemispherical volume of fluid directly above the RTD can be calculated with

$$R_{\text{Fluid}} = \frac{1/r_i - 1/r_o}{2\pi k_{\text{Water}}} \tag{2}$$

where  $r_i = \sqrt{l_m^2/2\pi}$  is the inner hemisphere radius,  $r_o = \sqrt{3l_m^2/2\pi}$  is the radius of the outer hemisphere, and  $k_{\text{Water}}$  is the thermal conductivity of water (0.6  $\text{W}/\text{m K}$ ) (Incropera and DeWitt 1996).

The thermal resistance due to convection from fluid moving within the microchannel must also be calculated. Determining the thermal resistance of convection first requires calculating a convection coefficient,  $h_x$ , that represents the local environment. The coefficient  $h_x$  depends on multiple factors and can be calculated by

$$h_x = \frac{0.453k_{\text{Water}}Re^{1/2}Pr^{1/3}}{x \left[ 1 - \left( \frac{\xi}{x} \right)^{3/4} \right]^{1/3}} \tag{3}$$

where  $Re$  is the Reynolds number,  $Pr$  is the Prandtl number, and  $\xi$  is the distance between the edge of the membrane and the heater (van der Wiel et al. 1993; Incropera and DeWitt 1996). The thermal resistance can then be found by integrating  $h_x$  over the membrane length using the formula

$$R_{\text{Convection}} = \frac{1}{l_h \int_{\xi}^{\xi+l_h} h_x dx} \tag{4}$$

To calculate the overall thermal resistance of the TPD, all three resistances are added in parallel:

$$R_{\text{Total}} = \frac{1}{\frac{1}{R_{\text{Fluid}}} + \frac{1}{R_{\text{Membrane}}} + \frac{1}{R_{\text{Convection}}}} \tag{5}$$

When a bead flows past the RTD, it changes  $R_{\text{Fluid}}$  and  $R_{\text{Convection}}$  because its thermal conductivity and specific heat are different from the fluid. The thermal conductivity of the bead,  $k_{\text{Bead}}$ , combines with the thermal conductivity of the water,  $k_{\text{Water}}$ , to form a composite thermal conductivity,  $k_c$ . We used effective medium theory (EMT) to model the change in average thermal conductivity caused by a bead suspended in a volume of fluid (Karayacoubian et al. 2005). The composite thermal conductivity,  $k_c$ , of the volume directly above the RTD can be calculated with

$$k_c = k_{\text{Water}} \frac{k_{\text{Bead}}(1 + 2\phi_{\text{Bead}}) - k_{\text{Water}}(2\phi_{\text{Bead}} - 2)}{k_{\text{Water}}(2 + \phi_{\text{Bead}}) + k_{\text{Bead}}(1 - 2\phi_{\text{Bead}})} \tag{6}$$

where  $k_{\text{Water}}$  is the thermal conductivity of water,  $k_{\text{Bead}}$  is the thermal conductivity of the bead, and  $\phi_{\text{Bead}}$  is the volume fraction of the bead within the heated volume.

The composite specific heat of the fluid volume,  $C_{p,c}$ , above the RTD can be calculated with

$$C_{p,c} = C_{p,\text{Water}}(1 - \phi_{\text{Bead}}) + C_{p,\text{Bead}}\phi_{\text{Bead}} \tag{7}$$

where  $C_{p,\text{Water}} = 4.184 \text{ J}/\text{g K}$  is the specific heat of water and  $C_{p,\text{Bead}}$  is the specific heat of the polystyrene bead. Neither supplier of the beads could provide thermal data so we assumed  $k_{\text{Bead}} = 0.168 \text{ W}/\text{m K}$  and  $C_{p,\text{Bead}} = 1.9 \text{ J}/\text{g K}$  for the model.

After  $k_c$  is calculated, it replaces the  $k_{\text{Water}}$  value in Eqs. 2 and 3. The composite specific heat  $C_{p,c}$  is used to recalculate the  $Pr$  number, which is used in Eq. 3. A new  $R_{\text{Total}}$  is calculated with these substituted values using

Eq. 5, which represents the new thermal resistance due to the bead.

The temperature change caused by the passing bead is calculated using an energy balance that equates the energy entering the system from Joule heating to the heat flow out of the system via conduction and convection. The equation for the energy balance is (Lee et al. 2008)

$$\frac{\Delta T}{R_{\text{Total}}} = I^2 Z(1 + \alpha \Delta T) \quad (8)$$

where  $\Delta T$  is the change in temperature within the system,  $Z$  is the electrical RTD resistance at room temperature,  $I$  is the current supplied to the RTD by the multimeter, and  $\alpha$  is the temperature coefficient of resistance. A  $\Delta T$  value is calculated with and without a bead present, using the appropriate  $R_{\text{Total}}$  values as described previously. The difference between these two  $\Delta T$  values gives the predicted temperature change as a bead passes.

The lumped model neglects thermal capacitance effects for simplicity. Thermal response times for the components of the TPD are on the order of 20 ms, so it is reasonable to assume that the system is at steady state. As discussed later, this assumption is valid except at high flow rates.

### 3 Materials and methods

#### 3.1 Device fabrication

The experimental setup is illustrated in Fig. 2. Microchannels were made out of the elastomer polydimethylsiloxane (PDMS) using standard micromolding procedures (Duffy et al. 1998). Briefly, SU8-2100 photoresist was spin-coated on a silicon wafer to a height of 250–300  $\mu\text{m}$  and then soft-baked. A high-resolution film mask was used to pattern microchannels in the SU8-2100. After a hard bake, the master was developed to reveal a positive relief of the microchannels. PDMS was mixed in a 10:1 elastomer-to-crosslinker ratio, degassed, and poured over the master and cured at 80  $^{\circ}\text{C}$  for 2.5 h. After curing the PDMS, it was carefully peeled from the wafer and diced, and ports were cored using a blunt 17-gauge syringe needle on one end of the microchannel and a 3-mm-diameter cork borer on the other end. The larger hole was used as a reservoir for depositing samples. Tubing was inserted into the smaller hole and connected to a syringe pump which was used to withdraw the fluid. The PDMS was then placed on the silicon substrate containing the RTD to form a watertight reversible seal. Typical microchannel dimensions were 300  $\mu\text{m}$  (W)  $\times$  300  $\mu\text{m}$  (H)  $\times$  8 mm (L).

The RTD was fabricated using traditional silicon microfabrication procedures. A silicon wafer was coated with a low-stress SiN film using low-pressure chemical

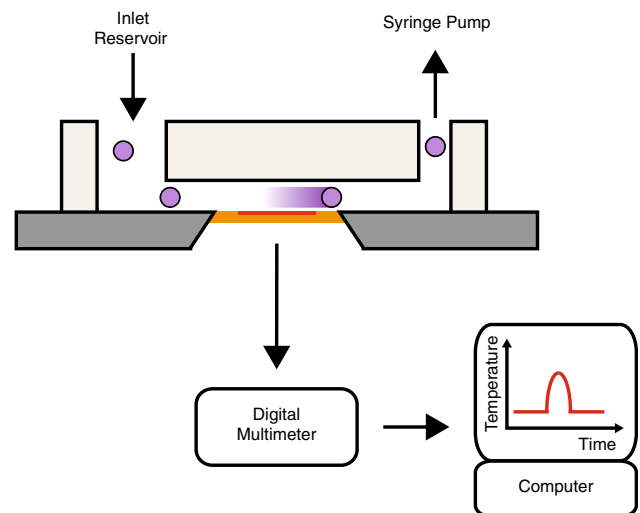


**Fig. 2** Overview of the experimental setup. Beads that flow past the RTD cause small changes in temperature, which are recorded via a LabView program

vapor deposition (LPCVD). The SiN was then patterned with AZ5214 and etched by a reactive ion etch (RIE). The exposed backside of the silicon was etched in a 30 % KOH bath at 60  $^{\circ}\text{C}$ . The KOH etch is an anisotropic and self-terminating etch and resulted in a well-defined 300  $\mu\text{m}^2$  SiN membrane that was 500 nm thick. A liftoff process was then used to pattern the Ni RTD and contact pads on the SiN membrane. The RTD and contact pads were patterned using AZ5214 image reversible photoresist followed by thermal evaporation of Ni metal film (30 nm thick) on the SiN membrane. The RTD was completed after liftoff of the metal in MicroChem 1,165 solvent. The resistance of the RTD was always about 1,500  $\Omega$ .

#### 3.2 Temperature measurement

The temperature of the Ni RTD was calculated using the equation

$$\Delta Z = Z_0(1 + \alpha \Delta T) \quad (9)$$

where  $\Delta Z$  is the measured change in resistance,  $Z_0$  is the resistance at room temperature,  $\alpha$  is the temperature coefficient of resistance for Ni, and  $\Delta T$  is the change in temperature. A HAAKE thermal bath was used to calibrate the RTD and calculate  $\alpha$ . To prevent self-heating of the RTD during calibration, a 0.1 mA current was applied to the RTD. Typical RTD linearity was excellent ( $R^2 = 0.9999$ ). However, the temperature coefficient of resistance,  $\alpha$ , was consistently about  $3 \times 10^{-3} \text{ K}^{-1}$ , which is lower than values reported in the literature ( $6 \times 10^{-3} \text{ K}^{-1}$ ) (Lacy 2011). Because  $\alpha$  is a function of the ratio of film thickness to the mean free path of electrons in metals, the lower  $\alpha$  value is likely due to the graininess of the evaporated thin

(30 nm) Ni film, which is comparable to the mean free path of electrons in typical metals (Jin et al. 2008; Leonard and Ramey 1966). Increasing the thickness of the Ni film should increase  $\alpha$ .

Temperature measurements were made in the TPD by mounting it in a custom jig that contained pogo pins to make contact with the Ni pads on the Si substrate. The pogo pins were then connected to a Keithly 2400 SourceMeter, which measured the RTD resistance using a 4-point measurement. Resistance values were recorded to a computer via GPIB and a custom LabView program. The 1 mA sourcing current from the SourceMeter through the RTD resulted in 1.5 mW of Joule heating. The steady-state temperature within the TPD at room temperature showed excellent stability.

The predicted Johnson noise of the resistor was 20  $\mu\Omega$  for the measurement bandwidth, but the lower limit of detection was determined by the SourceMeter which had a resolution of 10 m $\Omega$  (2 mK). Experiments showed that the system was capable of reliably measuring changes in resistance as low as 8 m $\Omega$  (1.8 mK) on a RTD with a nominal resistance of 1,500  $\Omega$ .

### 3.3 Sample preparation

Polystyrene beads 90  $\mu\text{m}$  (Polysciences) and 200  $\mu\text{m}$  (Corpuscular) in diameter were used to validate the TPD device. Since polystyrene has a density slightly higher than water ( $\approx 1.04 \text{ g/cm}^3$ ), we suspended beads in a mixture of DI water and glycerol to match the bead density. This mixture prevented beads from settling quickly and made it easier to flow multiple beads into the microchannel.

## 4 Results and discussion

Figure 3 shows the predicted temperature change as a function of bead diameter and thermal conductivity. A bead creates a temperature difference proportional to its diameter assuming it has a thermal conductivity different from the carrier fluid. The white dashed lines show the theoretical detection limit for the Keithly SourceMeter. For a polystyrene bead, the minimum detectable diameter is about 25  $\mu\text{m}$ . Our experiments support this prediction as we were not able to detect beads with diameters of 5, 10, and 15  $\mu\text{m}$ . A TPD with smaller membrane and microchannel dimensions would be able to detect these smaller beads because the device sensitivity depends on the ratio of the bead size to the heated fluid volume within the channel.

The thermal conductivity of the bead determines the magnitude of the temperature change. In the device we tested, the thermal conductivity threshold was

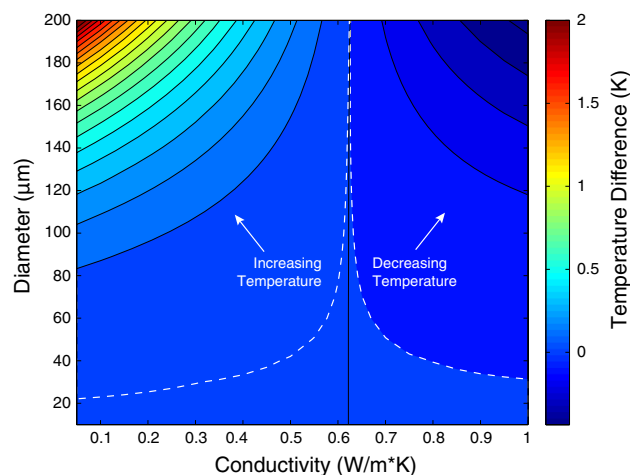


**Fig. 3** Contour plot of the lumped model showing the effect of bead diameter and thermal conductivity on the predicted temperature difference. The model assumes a volumetric flow rate of 5  $\mu\text{l/min}$  in a channel with a cross-section of 300  $\mu\text{m}^2$ . The dashed lines show the theoretical limit of detection for the device (2 mK). Black contour lines are drawn for each 0.1 K change

approximately 0.62 W/m $^2$ K. This threshold is a function of both the thermal conductivity of water and the convective heat transport within the device. A bead with a thermal conductivity higher than the threshold will generate negative temperature changes regardless of its size, while a bead with a thermal conductivity below the threshold will generate positive temperature changes. Thermally insulating beads like polystyrene generate a positive temperature change because they cause heat to build up near the RTD as they flow by. In contrast, thermally conductive beads such as those made from metal generate negative temperature changes because they rapidly conduct heat away from the RTD, resulting in a temperature drop.

The lumped thermal model predicts increases in RTD resistance (i.e., temperature) as polystyrene beads flow at a flow rate of 5  $\mu\text{l/min}$ : 0.09 K for a 90- $\mu\text{m}$  bead and 1.34 K for a 200- $\mu\text{m}$  bead. Figures 4 and 5 show representative traces for 90- and 200- $\mu\text{m}$  beads, respectively. The predicted temperature shift for the 90- $\mu\text{m}$  beads agrees well with the observed value of 0.5  $\Omega$ , or 0.11 K. Assumptions made about model parameters can explain the minor difference. For example, neither supplier of the beads could provide thermal conductivity data, so we used the thermal conductivity and heat capacity of regular polystyrene. The assumed thermal conductivity of SiN (16 W/m $^2$ K), which influences heat flow into the membrane, may also contribute to the difference between model and experimental results.

In contrast to the 90- $\mu\text{m}$  bead, the 200- $\mu\text{m}$  bead produces a 2  $\Omega$  decrease in resistance, or an equivalent change in temperature of  $-0.44 \text{ K}$ . The most likely explanation for this

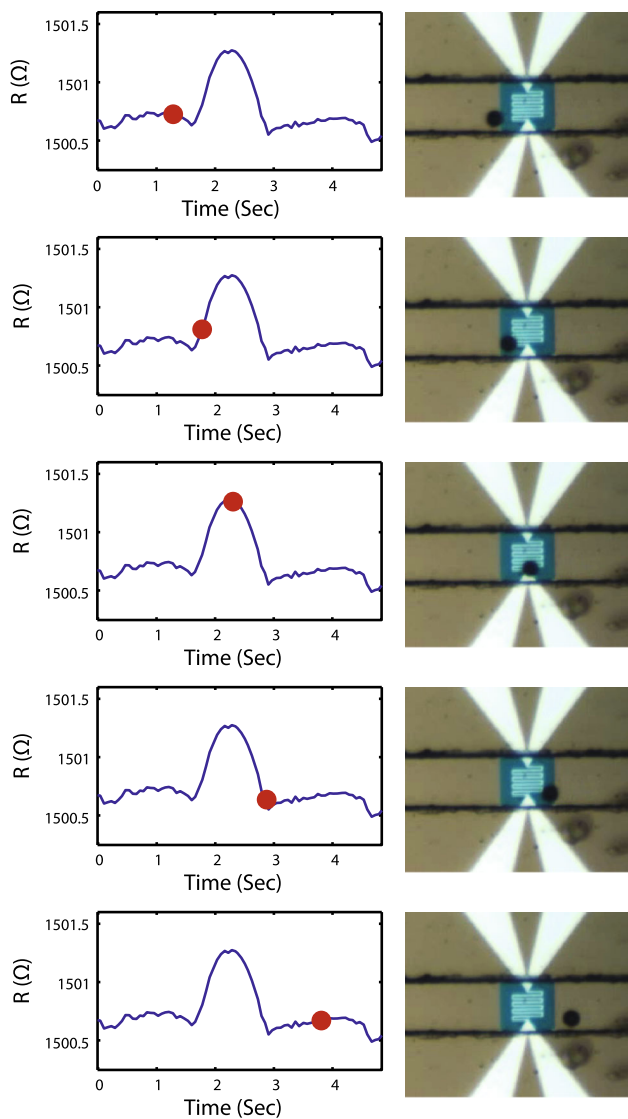


**Fig. 4** A representative plot showing the signal generated by a 90- $\mu\text{m}$ -diameter bead. Signals were consistently about  $0.5 \Omega$  ( $0.11 \text{ K}$ ) in amplitude

result is that the bead is altering the fluid velocity near the sensor. The membrane resistance cannot decrease nor can the resistance of the heated fluid volume directly above the sensor. The only remaining thermal resistance that can decrease is  $R_{\text{Convection}}$ . The model predicts that a velocity of  $10 \text{ mm/s}$  reduces the RTD temperature by  $2 \text{ K}$  compared to a velocity of  $0.01 \text{ mm/s}$  because of the increased heat transfer via convection. Therefore, velocity changes on the order of  $1 \text{ mm/s}$ , or less, will result in measurable decreases in RTD temperature. The velocity field around a sphere flowing a microchannel is known to be complex (Shardt et al. 2012). For example, it is likely that the bead is rotating due to the non-uniform flow field within the microchannel, which would enhance the cooling effect by increasing the local

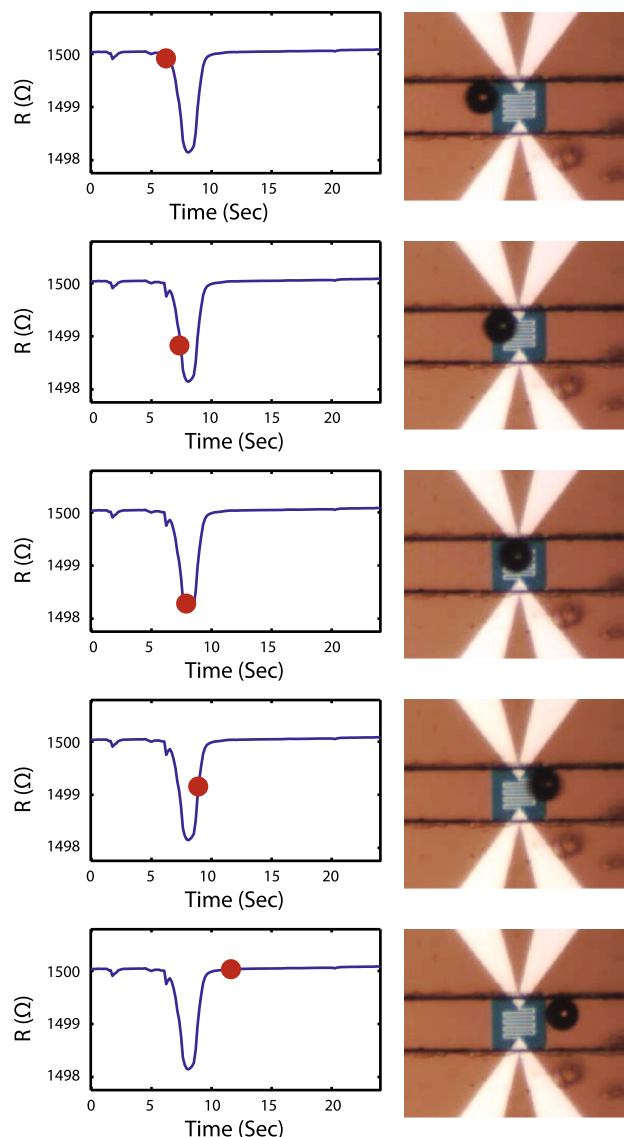


**Fig. 5** A representative plot showing the signal generated by a 200- $\mu\text{m}$ -diameter bead. Single beads of this size consistently generated negative peaks with amplitudes of about  $-2 \Omega$  ( $-0.44 \text{ K}$ )

velocity over the RTD. Thus, it is reasonable to assume that local velocity changes caused by the bead can yield negative temperature changes, even though the bead has a thermal conductivity lower than water. In contrast, the 90- $\mu\text{m}$ -diameter bead is smaller and perturbs the local flow field less than the 200- $\mu\text{m}$  bead, minimizing the velocity cooling effect, and yielding the expected increase in temperature.

Another prediction from the model is that the measured change in temperature is not affected by the distance of the bead from the sensor, assuming the bead is small enough to not significantly perturb the flow field. The thermal resistance of the water volume and bead are lumped together—the precise location of the bead does not impact the contribution of the bead to the overall thermal resistance. The

net result is the same: the temperature near the current source will increase if the thermal resistance of the fluid volume increases. However, the distance of the bead from the sensor will affect the thermal time constant of the system. The further away a bead is from the RTD, the larger the time constant is of the water between the RTD and bead. In practice, a longer time constant would increase the amount of time for the system to reach steady state, which would in turn limit how fast measurements can be made. Thus, the further the beads are away from the sensor, the slower the throughput. However, a key advantage of the TPD is that it can be made massively parallel because no cross talk exists between sensing channels.

As a proof-of-concept for particle counting, multiple beads were sequentially detected in the TPD using a flow rate of  $2 \mu\text{l}/\text{min}$ . Representative results are shown in Fig. 6. The beads all produced negative peaks of about  $2 \Omega$ , similar to the experimental results shown in Fig. 5. The beads are spaced about one sensor width ( $300 \mu\text{m}$ ) apart except for the last two, which are closer together. The results from this recording highlight the effect thermal capacitance has on throughput, namely that as beads become closer together there is less time for the system to reach steady state between beads resulting in peaks with reduced amplitude. The last two peaks have changes in resistance closer to  $1.5 \Omega$ . These results suggest that the TPD can count beads in two different ways. The first approach would be to simply count the number of passing particles. In this case, the relative amplitudes of the peaks are not important and the rate of counting can be high. However, accurate amplitudes might be needed to distinguish among multiple cell types or particles made of different materials. If these accurate measurements are needed, a second counting approach can be used. In this approach, a slower flow rate is used so that the system can reach steady state between peaks. The microscale dimensions and material properties of most particles mean that time constants are on the order of  $100 \text{ ms}$ , so counting rates would be limited to a few Hz per channel.

Lastly, we tested the effect of the carrier fluid on particle detection. We detected  $200\text{-}\mu\text{m}$ -diameter particles in glycerol, de-ionized (DI) water, and phosphate buffered saline (PBS), and the results are summarized in Fig. 7. Glycerol is an electrical insulator and was used to confirm that particle detection is due to thermal and not electrical sensing. The thermal and electrical conductivities of glycerol are lower than water which yields a higher baseline RTD resistance. Electrically conductive PBS is often used to suspend cells and other biological particles during counting. As shown by the representative trace in Fig. 7, a high salt concentration does not degrade the signal, but it

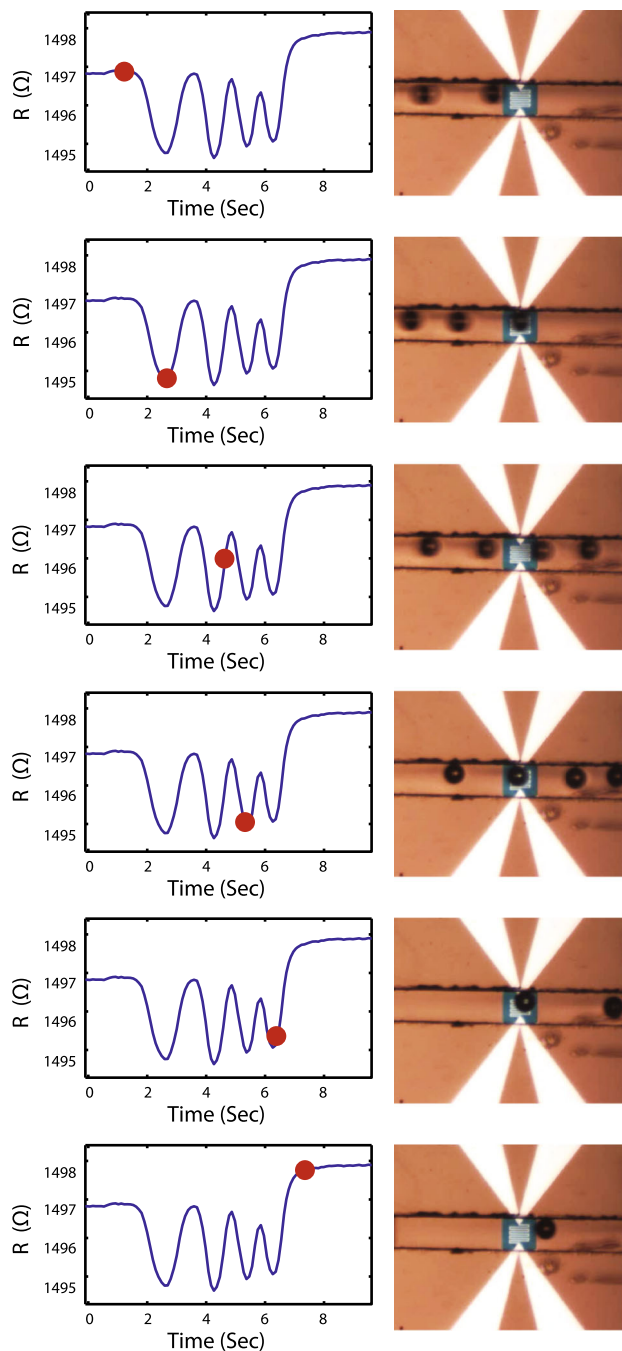


**Fig. 6** Multiple beads about  $300 \mu\text{m}$  apart were detected with the TPD. The amplitude of the last two beads is attenuated because they are closer together than the first two

does result in a slightly lower baseline RTD resistance. Even though saline is a good conductor of electricity, there is a negligible electrical potential within the device since only a single wire is used for sensing temperature. Furthermore, the RTD resistivity is orders of magnitude less than the resistivity of the fluids, so the geometric and material properties of the RTD will be the main

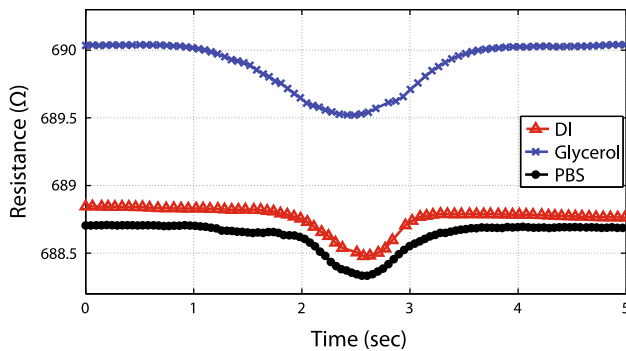


**Fig. 7** Beads 200  $\mu\text{m}$  in diameter were detected while suspended in glycerol, DI water, and PBS. A slower flowrate was used for glycerol, resulting in a broader peak as the bead flowed past the sensor

determinant of the baseline RTD resistance. The TPD works with fluids that possess a variety of thermal and electrical conductivities, which broadens its range of possible applications.

## 5 Conclusions

In summary, we have demonstrated a new device for detecting and counting particles based on thermal measurements. We have developed a first-order lumped model to explain the measured results. The size of the particles detected was roughly one-third of the sensor, but the principle can be used to detect particles of other sizes. We anticipate using this device to count other particles of interest, most notably biological cells, where it could be used in conjunction with, or a replacement for, flow cytometers. We also envision that the TPD can be used to thermally characterize particles as they flow by, opening up a new dimension in the high-throughput characterization of single cells.

**Acknowledgments** We thank Clement Kleinstreuer and John Sader for helpful discussions.

## References

- Duffy DC, McDonald JC, Schueller OJA, Whitesides GM (1998) Rapid prototyping of microfluidic systems in poly(dimethylsiloxane). *Anal Chem* 70(23):4974–4984
- Incropera FP, DeWitt DP (1996) Fundamentals of heat and mass transfer, 4th edn. Wiley, New York
- Janes MR, Rommel C (2011) Next-generation flow cytometry. *Nat Biotechnol* 29(7):602–604
- Jin JS, Lee JS, Kwon O (2008) Electron effective mean free path and thermal conductivity predictions of metallic thin films. *Appl Phys Lett* 92(17):171910
- Karayacoubian P, Bahrami M, Culham JR (2005) Asymptotic solutions of effective thermal conductivity. In: Proceedings of IMECE 2005. ASME international mechanical engineering congress and exposition. Orlando, Florida, USA, IMECE2005-82734
- Lacy F (2011) Evaluating the resistivity-temperature relationship for RTDs and other conductors. *IEEE Sens J* 11(5):1208–1213
- Lee J, Spadaccini C, Mukerjee E, King W (2008) Differential scanning calorimeter based on suspended membrane single crystal silicon microhotplate. *J Microelectromech Syst* 17(6):1513–1525
- Leonard WF, Ramey RL (1966) Temperature coefficient of resistance in thin metal films. *J Appl Phys* 37(9):3634–3635
- Murali S, Jagtiani AV, Xia X, Carletta J, Zhe J (2009) A microfluidic coulter counting device for metal wear detection in lubrication oil. *Rev Sci Instrum* 80(1):016105
- Shardt O, Mitra SK, Derksen J (2012) Lattice boltzmann simulations of pinched flow fractionation. *Chem Eng Sci* 75(0):106–119
- van der Wiel A, Linder C, de Rooij N, Bezinga A (1993) A liquid velocity sensor based on the hot-wire principle. *Sens Actuators A Phys* 37(38(0):693–697
- Yi N, Park BK, Kim D, Park J (2011) Micro-droplet detection and characterization using thermal responses. *Lab Chip* 11:2378–2384
- Zhang H, Chon C, Pan X, Li D (2009) Methods for counting particles in microfluidic applications. *Microfluid Nanofluid* 7(6):739–749